ACS APPLIED NANO MATERIALS

www.acsanm.org Article

Dextran-Gold Nanoparticle-Based Tablets and Swabs for Colorimetric Detection of Urinary H_2O_2

Zubi Sadiq, Muna Al-Kassawneh, Seyed Hamid Safiabadi Tali, and Sana Jahanshahi-Anbuhi*

Cite This: https://doi.org/10.1021/acsanm.4c05691 Read Online

ACCESS | Metrics & More | Article Recommendations | Supporting Information

ABSTRACT: Diagnosis of oxidative stress is essential to avoiding serious life-threatening situations. Hydrogen peroxide (H_2O_2) is a potential biomarker of oxidative stress. Herein, we introduce a reagent-free nanoscale approach for the colorimetric detection of urinary H_2O_2 utilizing dextran-gold nanoparticles (dAuNPs). The plasmonic properties of these nanoparticles are central to their function, leveraging their high surface area and tunable optical characteristics for sensitive detection. We transformed the colloidal dAuNPs solution into two formats: as a tablet (dAuNPs-Tablet) or impregnated on a cotton swab (dAuNPs-Swab). The assay generates a hydroxyl radical (•OH) from H_2O_2 via the Fenton reaction, followed by nanoscale-driven detection of H_2O_2 using a plasmonic tablet and swab sensors. In the presence of H_2O_2 in a sample, the red color of the tablet solution or plasmonic swab turns to blue due to salt-induced nanoparticles aggregation. The transition in color is observed due to •OH-assisted degradation of the dextran layer around dAuNPs, leading to the loss of colloidal stability and subsequent aggregation of dAuNPs. Sodium chloride acts as the aggregating agent, enhancing the nanoscale interactions. The detection limit in artificial urine is found to be 50 μM for the tablet sensor and 100 μM for the swab sensor. The plasmonic tablet is more stable as compared to a plasmonic swab which gradually loses stability, after one month, with approximately 40% degradation within three months. Interference studies demonstrate the high selectivity of both platforms for H_2O_2 detection. Notably, we investigated the H_2O_2 levels in human urine samples from healthy volunteers (both female and male) before and after green tea consumption. The observed decrease in the H_2O_2 level in urine postgreen tea consumption suggests a potential role of green tea antioxidants in mitigating oxidative stress. The utilization of nanoprobes in our research not only enhances our understanding of oxidative stress dynamics but also drives advancements in point-of-care detection platforms, offering enhanced portability and ease of use of nanoprobes. These platforms open exciting avenues in healthcare diagnosis.

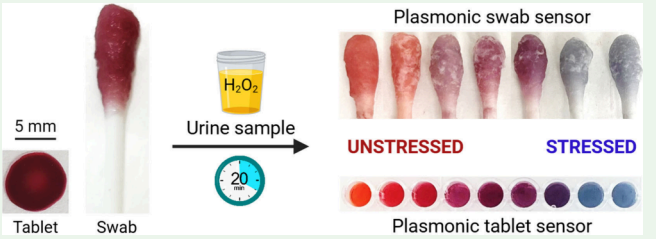

KEYWORDS: *Gold nanoparticles, hydrogen peroxide, Fenton reaction, tablet sensor, plasmonic swab, oxidative stress*

1. INTRODUCTION

Oxidative stress is an imbalance between the production or accumulation of reactive oxygen species (ROS) and the detoxification ability of antioxidants or biological systems because of poor dietary habits or the body's own metabolic functions.[1] The increased level of oxidative stress is associated with several metabolic disorders (e.g., diabetes, kidney damage),[2] neurodegenerative illnesses (e.g., Alzheimer's disease, Parkinson's disease),[3] cardiovascular conditions (e.g., heart failure),[4] and cancer.[5] Therefore, timely monitoring of oxidative stress is highly important to avoid life-threatening conditions. Various biomarkers for oxidative stress include end-products of oxidative damage to different biomolecules such as 8-hydroxy-2-deoxyguanosine (8-OHdG),[6] malondialdehyde (MDA),[7] 3-nitrotyrosine,[8] or explicit determination of oxygen radical production such as aromatic hydroxylation[9] or spin trapping.[10] As oxidative stress is not routinely tested in the clinical laboratory, the majority of these biomarkers relies on mass spectrometry and electron spin resonance spectroscopy or uses HPLC-based determination.[11] Considering these limitations, hydrogen peroxide (H_2O_2) as a whole-body oxidative stress biomarker has been highlighted in the literature.[12,13] Various biological samples, such as exhaled breath, sweat, blood, and urine, release different levels of H_2O_2. Among these, urine is an attractive medium for point-of-care applications due to its easy and noninvasive collection. The urinary H_2O_2 level varies drastically in healthy individuals with an average value of 100 ± 60 μM.[14] However, this level is increased up to 3-fold in different patients (e.g., cancer, diabetes).[15] Similarly, a raised level of urinary H_2O_2 is associated with oxidative stress which can be lower using antioxidant therapy.[16]

Received: October 7, 2024
Revised: December 24, 2024
Accepted: January 2, 2025

https://doi.org/10.1021/acsanm.4c05691
ACS Appl. Nano Mater. XXXX, XXX, XXX−XXX

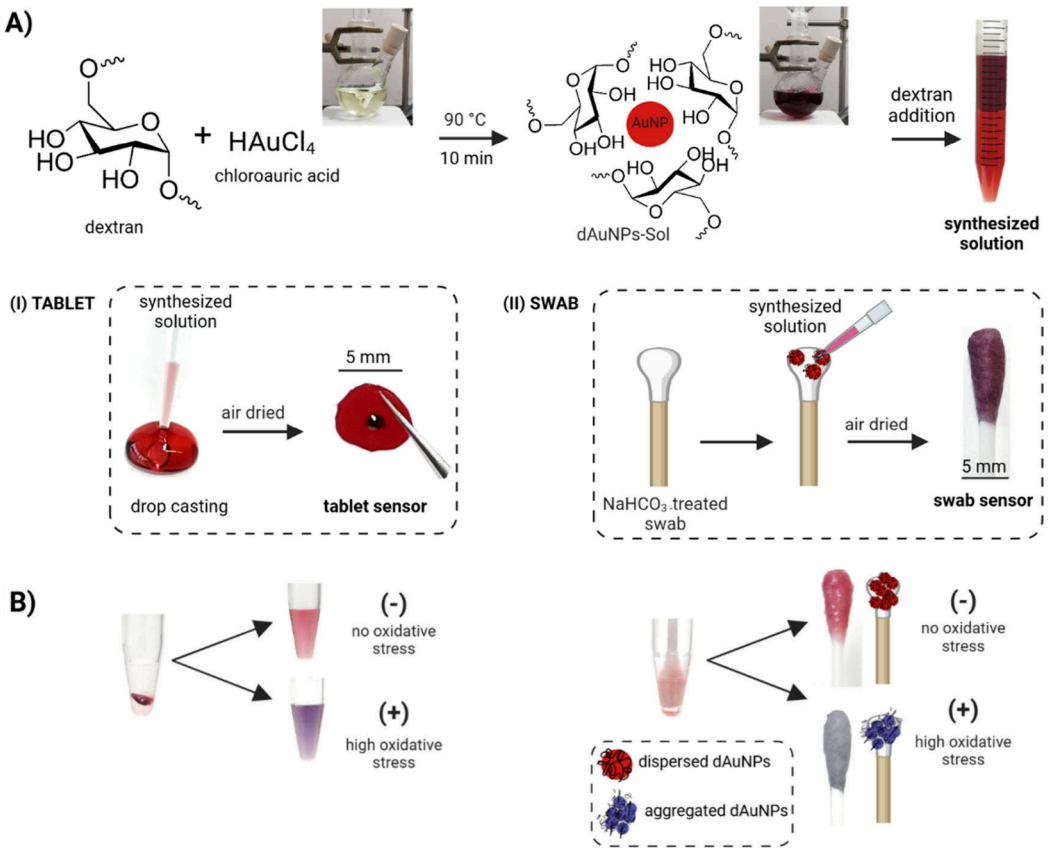

Figure 1. Synthesis of dextran-gold nanoparticles (dAuNPs) colloidal solution followed by tablet and swab sensor formation for the colorimetric detection of hydrogen peroxide (H_2O_2) as an oxidative stress biomarker. **A)** The dAuNPs solution was synthesized using chloroauric acid as a source of gold atoms and dextran as a reducing and stabilizing agent (yellow mixture in a flask). The dAuNPs-Sol (wine-red solution in a flask) was then mixed with dextran postsynthetically to get the plasmonic probe solution. This probe solution was used to cast the (I) tablet via the drop casting technique and was also (II) poured onto the alkaline-treated swab; **B)** The plasmonic tablet and swab sensors were utilized to measure the concentration of urinary H_2O_2 based on the Fenton reaction, where a blue color readout indicates a high level of oxidative stress.

Fenton chemistry has a well-known standing for H_2O_2 detection in the presence of low-valency transition metal ions (i.e., Cu^{1+}, Fe^{2+}, Cr^{3+}).[17] Fenton reagents (i.e., H_2O_2 and Fe^{2+}) generate a hydroxyl radical (•OH) which is a strong oxidizer with +2.80 V oxidation potential, which is slightly inferior to fluorine oxidation potential (+2.87 V).[18] This •OH can react with a variety of organic compounds leading to either degradation of these compounds or their conversion into less toxic products.[19] Moreover, the •OH initiates macromolecular damage in proteins, DNAs, and lipids causing cell damage.[1] Further, the •OH species is related to the detection of H_2O_2 because H_2O_2 is the precursor of •OH. Thus, the detection of H_2O_2 through the Fenton reaction is the center of attraction for scientific research. Fenton-mediated detection of H_2O_2 such as the ferrous ion−o-dianisidine complex (TOS-dianisidine) assay, ferric-xylenol orange (FOX) assay, and reactive oxygen metabolites derived compounds (d-ROMs) assay either uses the carcinogenic substance, requires longer incubation periods and centrifugation steps, or has a high tendency of false results.[20] Hence, there is a need for new methodologies as well as improvement in existing approaches for H_2O_2 detection.

The H_2O_2 detection assays utilizing Fenton reagents and nanomaterials are both straightforward and cost-effective, providing a colorimetric read-out and portability for enhanced convenience.[21] A variety of nanomaterials such as silver nanoparticles (AgNPs),[22] platinum nanoparticles (PtNPs),[23] copper oxide nanoparticles (CuONPs),[24] graphene composite,[25] and gold nanoparticles (AuNPs)[26] have been employed for H_2O_2 detection. Among these, AuNPs have been well-explored due to their superior optical, catalytic, and photothermal conversion properties besides their high surface-to-volume ratio, easy preparation, and multifunctional surface modifications.[27−33] The H_2O_2 detection with AuNPs-based sensors has been reported with instrument-dependent techniques as well as portable methods. Instrument-dependent techniques include spectrophotometry, fluorometry, electroanalysis, chemiluminescence, resonance light scattering assays, and chromatography.[34−36] For portable methods, colorimetric readout receives considerable attention due to allowing for an easy, low-cost, and user-friendly assay. The AuNPs-related portable detection platforms could be based on substrates such as paper, textile fabric, synthetic polymer, thread, tablet, or swab that require an ultralow volume of the sample.[27,37,38] In such systems, quantification can be achieved through RGB color intensities using smartphone imaging.[39] Overall, the detection of H_2O_2 using AuNPs is important for the development of point-of-care sensors.

Lin et al. detected H_2O_2 using DNA-modified AuNPs where the hydroxyl radical was used to break the phosphodiester bonds in DNAs and decreased the quantity of DNAs on the surface of AuNPs causing their aggregation.[40] However, this assay required extensive pretreatment of DNA before the detection step. For example, the reduction of thiol-modified

https://doi.org/10.1021/acsanm.4c05691
ACS Appl. Nano Mater. XXXX, XXX, XXX−XXX

oligo disulfide was time-consuming and required −20 °C conditions to prepare and store the reduced thiol-DNA followed by 16 h of stirring in the dark to adsorb the thiol-DNAs onto AuNPs. In another study, Wu et al. detected H_2O_2 through the aggregation of AuNPs because H_2O_2 treatment removed polyethylene glycol chains from the AuNPs surface that exposed inner hydrophobic ligands, causing AuNPs aggregation in water.[41] Again, this method required up to 28 h for the detection of H_2O_2 in a dynamic μM range. Hence, there is a need to introduce a new detection strategy which is simple, portable, quick, user-friendly, and cost-effective. Our group has a solid background in the tablet-based detection platform used for various applications.[27,42−46] We fabricated a tablet sensor by encapsulation of AuNPs used for the detection of acid-labile groups.[27] Additionally, our team has developed pullulan stabilized AuNPs-based tablet sensors for detecting glucose and cysteamine through the expression and inhibition of peroxidase-mimetic behavior, respectively.[42,46]

Herein, we developed the plasmonic tablet and swab sensors for point-of-care detection of oxidative stress biomarkers using urinary H_2O_2. Both the tablet and swab sensors were prepared from dextran-gold nanoparticles solution (dAuNPs-Sol). The synthesis of dAuNPs-Sol, along with the preparation of tablet and swab sensors, is illustrated in Figure 1A, while their colorimetric responses are presented in Figure 1B. These sensors underwent comprehensive characterization using techniques such as ultraviolet−visible and Fourier transform infrared (FTIR) spectroscopy, transmission electron microscopy (TEM), scanning electron microscopy (SEM), energy dispersive X-ray spectroscopy (EDS), zeta potential, and dynamic light scattering (DLS). The detection mechanism relies on the Fenton-assisted •OH radical generation, leading to the degradation of the polymeric layer surrounding dAuNPs and subsequent loss of colloidal stability. Sodium chloride (NaCl) was then employed as an aggregating agent to induce a visual color transition from red to blue. The observed color change directly correlated to the concentration of H_2O_2, offering an estimation of whole-body oxidative stress. Calibration curves were generated by plotting the H_2O_2 concentration against the aggregation/dispersion state of dAuNPs, utilizing *ImageJ* software for the tablet and swab sensors. Both sensors demonstrated high analytical performance in quantifying H_2O_2 levels. Unlike conventional chromogenic methods that are toxic and require a specific buffer for preparation, our approach leverages the unique plasmonic properties of dAuNPs for a clear color change upon hydroxyl radical interaction. Moreover, the assay's adaptability into portable formats, such as tablets and swabs, coupled with its long-term stability and high selectivity, highlights its practical advantages over traditional methods.

To assess the sensors' real-world applicability, urinary H_2O_2 concentration was measured as an oxidative stress biomarker in real urine samples collected from healthy male and female volunteers before and after a specific duration of consuming green tea. This evaluation not only showcased the performance of our plasmonic sensors in practical scenarios but also allowed us to observe the impact of diet on oxidative stress levels. Moreover, our sensors are promising for point-of-care applications, such as diagnosing kidney inflammation through ROS detection in human urine.

2. EXPERIMENTAL SECTION

2.1. Chemicals and Instrumentation. Tetrachloroauric acid ($HAuCl_4$, 30 wt % in dilute HCl), hydrogen peroxide (H_2O_2, 30 wt % or 9.8 M), ferrous sulfate heptahydrate ($FeSO_4{\cdot}7H_2O$), dextran (100 kDa), sodium phosphate monobasic monohydrate ($NaH_2PO_4{\cdot}H_2O$), disodium hydrogen phosphate (Na_2HPO_4), sodium bicarbonate ($NaHCO_3$), sodium chloride (NaCl), citric acid ($C_6H_8O_7$), sodium hydroxide (NaOH), ascorbic acid ($C_6H_8O_6$), and sulfuric acid (H_2SO_4) were purchased from Sigma-Aldrich. Zinc chloride ($ZnCl_2$) and copper chloride ($CuCl_2$) were purchased from Thermo Scientific Chemicals. Deionized water was used to prepare all of the solutions. Citrate-phosphate buffer was prepared using 0.2 M disodium hydrogen phosphate and 0.1 M citric acid. The final pH was adjusted by using citric acid. The ferrous sulfate solution was prepared in citrate-phosphate buffer. Artificial urine (99.99% purified) was obtained from Biochemazone, USA. The volunteers consumed Japanese green tea (sencha and matcha blend, Kirkland Signature brand) at a concentration of 1.5 g/200 mL water. Cotton swabs and a carbon steel tray (Betty Crocker) were purchased from a local Walmart store in Montreal, Canada. A vortex machine (model no. 9454FIALUS, 50/60 Hz, Fisher) was used to dissolve a tablet into a Fenton reagent. The morphology and chemical nature of dAuNPs were studied by transmission electron microscopy (TEM, Talos L120C, 20−120 kV) and scanning electron microscopy (SEM, Phenom ProX). SEM-EDS images were captured at 15 keV with solid samples cast on carbon grids. Absorption spectra of dAuNPs were recorded on a UV−vis spectrophotometer (BioTek, Cytation 5, imaging reader). The particle size analyzer (Litesizer 500, Anton-Paar, Austria) was used to record the hydrodynamic size of dAuNPs via the dynamic light scattering (DLS) technique. Surface charge on dAuNPs was measured in Ω-shaped polystyrene cuvettes, with zeta potential analyzed via electrophoretic light scattering using the cmPALS technique (European Patent 2735870). All samples were collected in triplicate. The nanogold tablets were dried at room temperature or 50 °C in a laboratory oven without forced air convection (Thermo Scientific, Model# PR30525G, USA). The $NaHCO_3$ soured cotton swabs after nanogold adsorption were dried at room temperature and stored in an airtight box until use. Images of swab and tablet sensors were captured using an iPhone 13 and analyzed with *ImageJ* software (National Institutes of Health, USA).

2.2. Fabrication of Plasmonic Tablet and Swab Sensors. The glassware was washed three times with deionized water after being cleaned with a fresh aqua regia solution. A colloidal solution of dextran-gold nanoparticles (dAuNPs-Sol) was synthesized as per the literature procedure with some modification.[47] In short, 25 mL of a 1 mM $HAuCl_4$ solution was stirred with 50 μL of a 5% dextran solution at 90 °C followed by the addition of 50 μL of a 1 M NaOH solution. The flask contents changed from light yellow to colorless, then light pink, and finally into a wine-red dispersion which confirmed the synthesis of dAuNPs. The concentration of the dAuNPs solution was estimated to be ∼4.6 nM by Beer's-Lambert law using a UV−vis spectrophotometer based on a calculated extinction coefficient (ε) of 2.4×10^8 M^{-1} cm^{-1} at 520 nm for 13 nm particles.[45] The nanogold solution after postsynthetic addition of 2% dextran powder was mixed for 1 min and transformed to tablets (dAuNPs-Tablets) according to our previously established protocols.[27,45] In short, a plasmonic tablet was created by pipetting 100 μL of the dAuNPs solution on a nonstick tray followed by air-drying overnight at ambient conditions of 20 °C and 45% indoor humidity. Fully dried tablets were collected from the tray and stored in a glass vial at room temperature.

Also, the dAuNPs-Swab sensor was prepared in two steps. Initially, commercial cotton swabs were boiled in a $NaHCO_3$ solution (25 mM) for 5 min to remove any hydrophobic compounds, including fats and waxes. The $NaHCO_3$ soured swabs were washed with deionized water five times or until obtaining a neutral pH (∼7) using pH paper. These swabs were oven-dried at 60 °C for 1 h followed by pouring a fixed volume (200 μL) of a nanogold solution onto each swab. The plasmonic swabs were air-dried for ∼8 h and stored in an airtight glass jar at room temperature until further use. Notably, a

https://doi.org/10.1021/acsanm.4c05691
ACS Appl. Nano Mater. XXXX, XXX, XXX−XXX

fixed concentration (~4.6 nM) and volume of dAuNPs were consistently used during tablet formation and swab preparation in each batch to prevent clumping and ensure consistency in the amount of dAuNPs across different tablets and swabs. A controlled drying environment, including regulated temperature and humidity, was also maintained to promote particle uniformity and prevent aggregation during solvent evaporation. However, even if nonuniform particle distribution occurs within a tablet or swab, it does not impact the results, as the entire tablet is dissolved in the Fenton reagent, giving the exact same concentration of dAuNPs and resulting in a consistent color change. Similarly, the entire swab is immersed in the Fenton reagent to generate the blue color for analysis.

2.3. Optimization Study and Reaction Kinetics of the Hydrogen Peroxide (H_2O_2) Assay. Reaction conditions were optimized to establish the experimental protocols for the H_2O_2 assay. Major operational parameters such as the amount of dextran in dAuNPs, concentration and pH of the ferrous sulfate solution, concentration and volume of sodium chlorite, and temperature of the reaction medium were investigated. Further, the Fenton-based •OH radical generation was confirmed by using ascorbic acid as a radical scavenger. For this, 1 mM ascorbic acid (10 μL) was incubated with Fenton's reagent for 10 min followed by the addition of a plasmonic tablet and NaCl solution. Finally, the reaction kinetics was studied using 1 mM H_2O_2 in the presence and absence of ascorbic acid.

2.4. Detection of H_2O_2 as a Potential Oxidative Stress Biomarker. *Fenton Reaction-Based Colorimetric Assay Using a Tablet Sensor.* The colorimetric detection of H_2O_2 based on Fenton chemistry is comprised of two steps; generation of free hydroxyl radical (•OH) and detection of H_2O_2 using the dAuNPs probe. The first step involves the Fenton reagent where a reaction between ferrous ions and H_2O_2 takes place to produce •OH. For this, 50 μL of different concentrations of H_2O_2 in water (30, 50, 100, 125, 250, 500, 700, and 1000 μM) was mixed with 10 μL of 3 mM ferrous sulfate (pH 3) followed by the addition of 200 μL of deionized water. This solution was incubated for 10 min to ensure the generation of •OH which participated in the detection step. In the second step, a plasmonic tablet (100 μL of dAuNPs) was added to the previously formed Fenton solution and vortexed to get a homogenized mixture. Finally, 30 μL of 1 M NaCl solution was added, and UV−vis spectra were collected after 10 min of incubation. Next, the H_2O_2 assay was employed in artificial urine using the same experimental protocols where artificial urine was spiked with different concentrations of H_2O_2 ranging from 30 to 1000 μM. The color change of the tablet solution was recorded as blue/red color intensity using *ImageJ* software in addition to measuring their absorbance intensity at λ_{520} and λ_{650} nm using a UV−vis spectrophotometer. Notably, for the analysis, a full well of the 96-well plate was selected as the region of interest in *ImageJ* to eliminate any inconsistencies in the color selection. Each experiment was conducted in triplicate to ensure reproducibility.

Fenton Reaction-Based Colorimetric Assay Using a Swab Sensor. A plasmonic swab was used for the colorimetric detection of H_2O_2 facilitated by Fenton chemistry in aqueous media and artificial urine samples. For this, 10 μL of 3 mM ferrous sulfate (pH 3), 200 μL of deionized−distilled water, and 50 μL of different concentrations of H_2O_2 (30, 50, 100, 125, 250, 500, 700, and 1000 μM) were incubated for 10 min followed by dipping of the dAuNPs-Swab in Fenton solution. Afterward, 30 μL of a 1 M NaCl solution dropped onto the swab. After 10 min, optical images of swabs were collected and analyzed by *ImageJ* software for any change in their color intensity. The RGB color analysis was used to plot a calibration curve for quantitative analysis. Similarly, for cotton swab analysis, the entire area of the swab was chosen as the region of interest, which minimized any discrepancies in color variation across the swab. This experiment was also performed in triplicate to confirm consistent and reliable results.

2.5. Interference Study Using a Plasmonic Tablet and Swab. Possible interferents that might exist in the urine sample are anions (Cl^-), cations (Na^+, K^+, NH_4^+, Mg^{2+}, Ca^{2+}, Zn^{2+}, and Cu^{2+}), glucose, uric acid, and ascorbic acid. These potential interferents were tested to check the selectivity of a plasmonic tablet and swab sensors toward H_2O_2 detection. The same experimental procedure was followed as mentioned in section 2.4 using 0.1 mM H_2O_2 in the presence of 1 mM anions and 0.1 mM cations and 0.1 mM glucose, uric acid, and ascorbic acid separately. The change in color intensity was estimated using *ImageJ* software for the plasmonic tablet and swab sensors.

2.6. Determination of Oxidative Stress in Male and Female Volunteers. The newly proposed H_2O_2 assay was utilized to measure the oxidative stress level in healthy individuals (male and female) before and after consuming 200 mL of green tea three times a day for a week. The volunteers did not take any drug, ergogenic aids, or antioxidant supplements for at least 10 weeks before the study. A standard literature method as reported by Halliwell et al. was followed to collect the urine samples.[48] These samples were spiked with known concentrations of H_2O_2 (160, 200, 250, and 500 μM) and quantitatively analyzed using a plasmonic tablet and a swab sensor following the same procedure as that mentioned in section 2.4. We use a buffer to ensure that variations in the sample's pH do not affect the sensor's performance. The recovery% (R%) and relative standard deviation% (RSD%) were calculated using their standard formula to show the practical applicability and precision of both plasmonic sensors.[42]

3. RESULTS AND DISCUSSION

3.1. Characterization of Plasmonic Sensors. In this section, we thoroughly explore the characterization of our plasmonic sensors, which are crucial for understanding their performance and mechanisms. Through a comprehensive analysis employing various spectroscopic and microscopic techniques, we studied the structural and functional properties of these sensors. This detailed characterization lays the groundwork for subsequent discussions on their efficacy in the detection of oxidative stress biomarkers. A colloidal solution of dextran-gold nanoparticles (dAuNPs-Sol) was prepared according to the literature method by reacting chloroauric acid with dextran in an alkaline medium.[47] Subsequently, dAuNPs-Sol was encapsulated as a tablet (dAuNPs-Tablet) or deposited on pretreated cotton swabs (dAuNPs-Swab) to fabricate plasmonic sensors. The dAuNPs from both solid platforms (tablet and swab) were released into deionized water to analyze their morphology and surface charge by employing UV−vis and FTIR spectroscopy, dynamic light scattering (DLS), transmission electron microscopy (TEM), and a zeta potential analyzer. Apart from solution phase characterization of nanoparticles, scanning electron microscopy (SEM) with energy dispersive X-ray spectroscopy (EDS) analysis of the solid plasmonic sample is reported herein, whereas we have already published atomic force microscopy (AFM) analysis of a solid tablet.[27]

A classical bottom-up approach employing a wet chemical reduction method opted for the one-pot NaOH-assisted synthesis of the dAuNPs solution. The gold chloric acid solution was refluxed in alkaline media with dextran as a reducing, stabilizing, and capping agent.[47] Generally, dextran oxidation is followed by $HAuCl_4$ reduction to produce aurous salt (AuCl) which undergoes a disproportionation reaction producing monomers for the formation of nanoparticles.[47] Alkaline media facilitated the formation of different gold complexes during the synthesis. The AuNPs were readily stabilized by copious alcohol hydroxyl groups of the dextran chain. Within 5 min, the color of the reaction medium was shifted from colorless (Au^{3+}) to light pink and finally to a burgundy/wine red (Au^0) transparent colloidal solution. The reaction was kept under the same conditions for an additional 30 min to ensure no further increase in the absorption intensity of dAuNPs-Sol. A sharp, narrow, and symmetrical absorption

https://doi.org/10.1021/acsanm.4c05691
ACS Appl. Nano Mater. XXXX, XXX, XXX−XXX

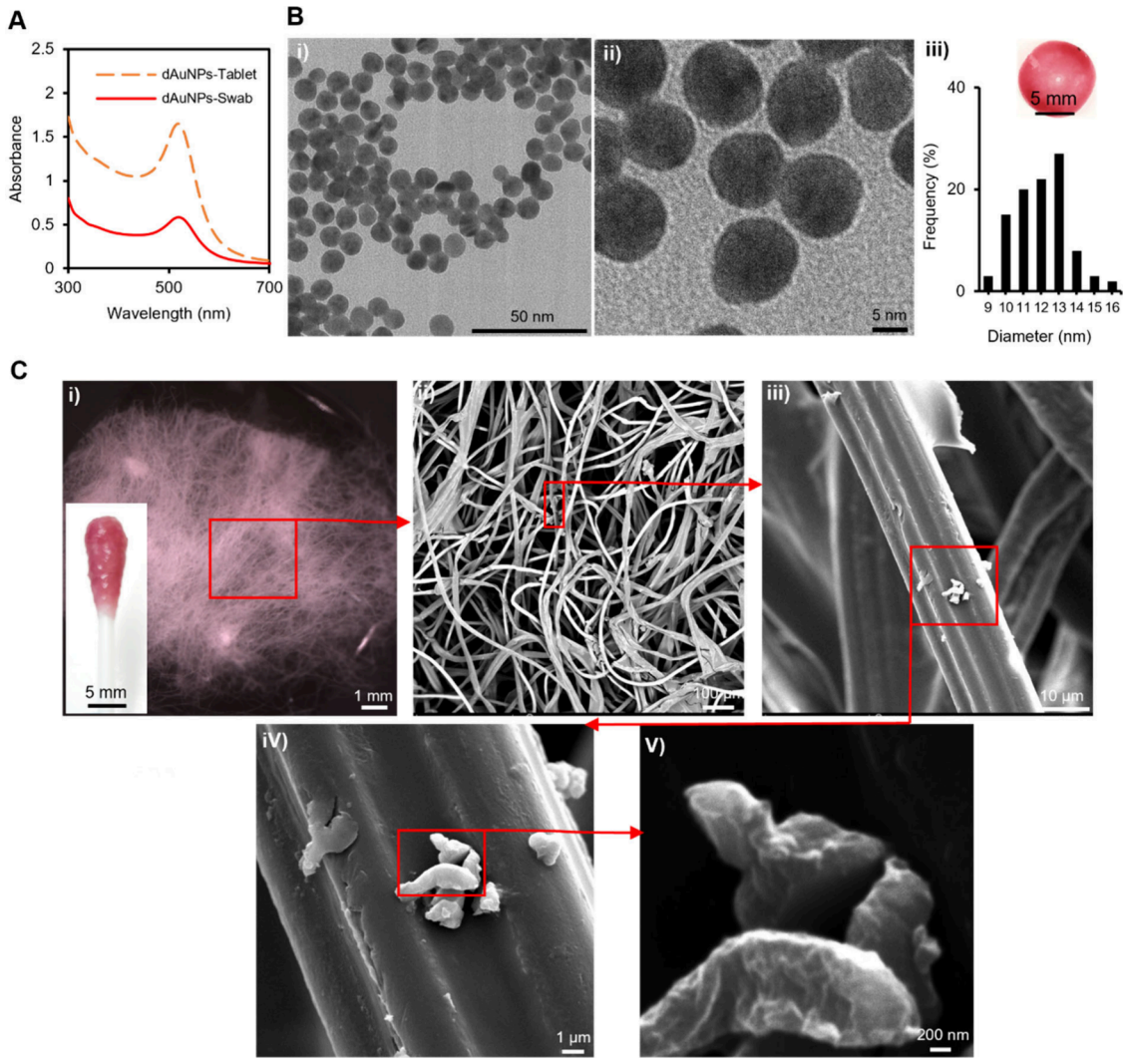

Figure 2. Characterization of gold nanoparticles in tablet and swab formats. **A)** Absorption spectra showing peak maxima at 520 nm for both the tablet and swab; **B)** The TEM image of the dAuNPs-Tablet shows (i) an average particle size of 12 ± 1 nm, (ii) the round shape of nanoparticles, and (iii) a particle distribution graph, with the optical image of a tablet shown as an inset; **C)** The SEM images of the dAuNPs-Swab show clusters of Au particles distributed within the cellulose fibers of the cotton swab at different scale bars: (i) 1 mm (with the optical image of the dAuNPs-swab shown as an inset), (ii) 100 μm, (iii) 10 μm, (iv) 1 μm, and (v) 200 nm.

band appeared at λ_{520} nm demonstrating monodispersed dAuNPs of 13 nm. FTIR spectrum has characteristic functional peaks of dextran and AuNPs solution as supported by the literature.[47] The hydrodynamic size was 35.02 nm (15% PDI), and the surface charge was −42.6 mV as shown by DLS and zeta potential analysis respectively (Figure S1).

The dAuNPs-Sol was mixed with pristine dextran (2%) to get the highly stabilized nanogold dispersion used to cast plasmonic tablets according to our previously established protocols.[27] The plasmonic swab was prepared by dropping the nanogold colloidal dispersion onto pretreated cotton swabs. Of note, aggregation of nanogold was observed when $NaHCO_3$-soured swabs were directly soaked in dAuNPs dispersion and dried. The reason for aggregation may be the adsorption of maximum nanogold particles; hence, a premeasured volume (200 μL) of dAuNPs dispersion was carefully pipetted out on alkaline treated swabs. However, if the same volume of the dAuNPs solution was pipetted out on untreated swabs, again, nanoparticles were aggregated on the surface of the cotton swab at random places due to the presence of the existing wax layer on the swab (Figure S2A). It is also important to mention that a cotton swab was preferred over different materials such as cotton balls, face-mask thread, cotton thread, and mouth floss because these materials did not adsorb nanogold efficiently and could not sustain them well-dispersed on the surface. All of these materials turned purplish-blue after drying, hence unsuitable to be used as a colorimetric probe (Figure S2B).

UV−vis extinction spectra of the dAuNPs-Tablet, dAuNPs-Swab, and dAuNPs-Sol are identical, indicating the post-synthetic addition of dextran in the dAuNPs solution did not change particle morphology in the tablet and swab. However, the decreased intensity of the peak in the swab as compared to the tablet was due to the partial release of dAuNPs into solution from the dAuNPs-Swab (Figure 2A). Of note, the surface of the $NaHCO_3$-scoured swab in neutral solutions is negatively charged due to dissociation of functional groups, such as hydroxyl and carboxyl groups as well as adsorption of dAuNPs from the solution, indicating the stability of gold particles on a swab.[49] Infrared analysis of dAuNPs in tablet and

https://doi.org/10.1021/acsanm.4c05691
ACS Appl. Nano Mater. XXXX, XXX, XXX−XXX

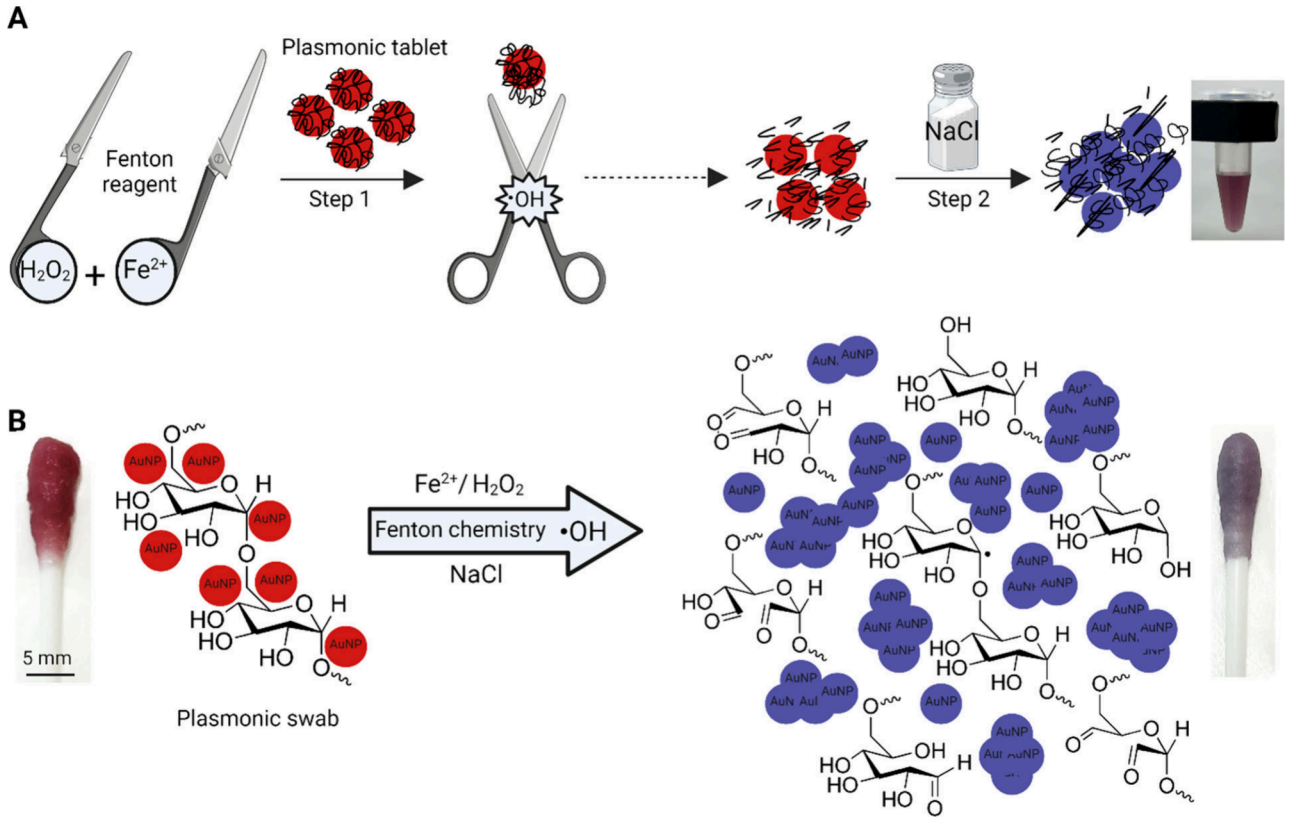

Figure 3. Fenton-mediated colorimetric detection of H_2O_2 via •OH-assisted degradation of dextran around dAuNPs resulting in aggregation of dAuNPs. **A**) A Fenton reagent consisting of H_2O_2 and ferrous ions (Fe^{2+}) produces an •OH radical which oxidizes dextran chains around dAuNPs in the first step. The oxidized dextran cannot protect dAuNPs fully and leads to the aggregation of particles upon the addition of sodium chloride in the second step, producing a red-to-blue color response; **B**) The red color of the plasmonic swab turns to blue aggregated particles by the influence of Fenton chemistry.

swab formats showed a peak at 1634 cm^{-1} corresponding to the C═O stretching frequency present in aldehyde groups which indicated the conversion of some of the dextran's hydroxyl groups into aldehyde functionality after oxidation, a process coupled with the reduction of Au^{3+} to Au^0 species.[50] The intense broadband at 3319 cm^{-1} suggested the presence of symmetrical stretching vibrations of hydroxyl functional groups (O−H), which might have arisen from alcoholic groups of dextran. The bands at 1150 and 997 cm^{-1} corresponded to the stretching vibrations of C−O bonds and α-glycosidic bonds (C−O−C) in dextran, respectively.[47] The absorption peak at 2925 cm^{-1} can be assigned to the −CH group stretching vibrations of dextran, which can be seen in the dAuNPs-Tablet and dAuNPs-Swab. The FTIR analysis showed the involvement of dextran in fabricating dAuNPs as well as surface attachment on nanogold particles (Figure S3).

The ζ-potential of the dAuNPs-Tablet and dAuNPs-Swab was estimated as −28.54 mV and −15.16 mV, respectively, which supports that the nanoparticle boundaries are well separated from the adjacent particles of a similar charge in the dispersion. These phenomena resist aggregation and confer stability of dAuNPs as tablet and swab platforms. The decrease in surface charge of the swab as compared to the tablet might be due to the partial release of nanogold particles in the solution, and most of the particles remained absorbed onto the swab surface. The hydrodynamic size of the dAuNPs-Tablets and dAuNPs-Swab was 160.6 nm (20% PDI) and 102.0 nm (33% PDI), respectively, as depicted from DLS analysis (Figure S3). The increased hydrodynamic size in the tablet solution as compared to the swab solution might be due to the efficient surrounding of solvent molecules around nanogold particles.[51] The increased size in both solid formats as compared to dAuNPs-Sol was due to the additional amount of the dextran polymer resulting in a thicker polymeric layer around dAuNPs leading to a bigger hydrodynamic size.[52] The surface morphology of a tablet and swab was characterized by TEM and SEM analysis, respectively, as shown in Figure 2. The average particle diameter of the tablet was 12 ± 1 nm with a round-shaped morphology observed in the TEM images (Figure 2B). The SEM micrographs of low and high magnifications (Figure 2C) depict the uniform distribution of dAuNPs aggregates (size in the tens of nanometers) on the cellulose fibers of the swab. EDS quantitative analysis confirmed the elemental composition of the dAuNPs-Tablet as 13.09% gold, 80.79% carbon, and 6.12% oxygen, while the dAuNPs-Swab consisted of 9.21% gold, 82.55% carbon, and 8.23% oxygen, as presented in Figure S3D.

3.2. Optimization Study for the H_2O_2 Assay. Next, we conducted an optimization study to refine the H_2O_2 assay methodology. By systematically investigating key parameters and experimental conditions, we aimed to enhance the sensitivity, accuracy, and reliability of our detection approach. Several influencing parameters such as the concentration of dextran in the dAuNPs suspension (0.01 or 2.01%), concentration of ferrous ion (Fe^{2+}) in the Fenton reagent, and amount of NaCl salt, pH, and temperature of the reaction medium were optimized in a univariate approach for the H_2O_2 assay as shown in Figure S4. The dAuNPs-Tablet solution is

https://doi.org/10.1021/acsanm.4c05691
ACS Appl. Nano Mater. XXXX, XXX, XXX−XXX

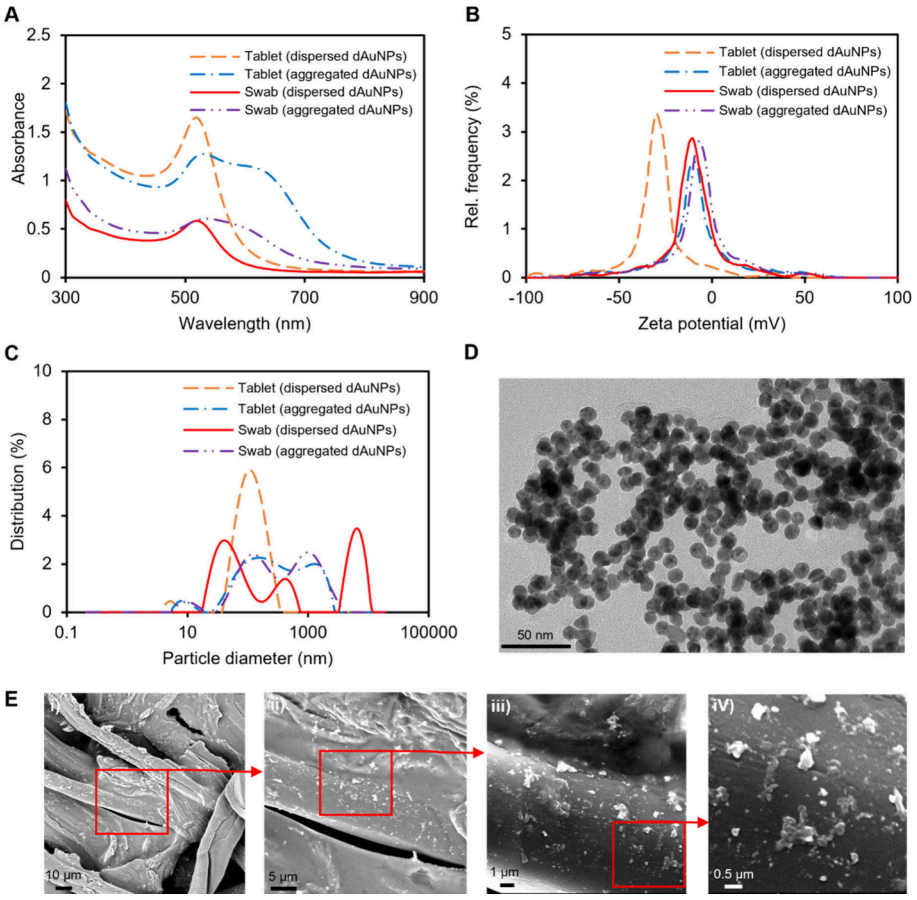

Figure 4. Comparison of the dAuNPs probe before (dispersed) and after (aggregated) detection of H_2O_2. **A**) Absorption spectra; **B**) A graph of zeta potential values; **C**) A plot of hydrodynamic size; **D**) A TEM image of the tablet-based assay solution after nanoparticles aggregation; and **E**) SEM images of the dAuNPs-swab after aggregation, shown at different scales; (i) 10 μm, (ii) 5 μm, (iii) 1 μm, and (iv) 0.5 μm.

more stable as compared to "as-synthesized" dAuNPs-Sol because of having 2% additional dextran powder which stabilized nanoparticles more effectively. The addition of Fe^{2+} or H_2O_2 alone caused no aggregation in the dAuNPs-Tablet but a slight decrease in peak intensity in the case of H_2O_2 (Figure S4A, curves b and e). Next, different concentrations of ferrous sulfate (1, 2, 3, and 6 mM) were tested with the dAuNPs-Tablet to choose the best concentration that could not induce aggregation in the dAuNPs-Tablet. The highly concentrated ferrous sulfate solution (6 mM) induced aggregation in the dAuNPs-Tablet, hence unsuitable for the assay.

The dAuNPs-Tablet withstands high ionic strength as previously reported by our group.[27] A different volume (10–50 μL) of the 1 M NaCl solution was incubated with the dAuNPs-Tablet solution for 10 min which showed no visible color change until 30 μL of NaCl. Thus, 30 μL of NaCl was chosen to enhance the signal read-out in H_2O_2 detection. Further, 100 μM H_2O_2 in the presence of 1–3 mM ferrous sulfate was used to generate the •OH radical followed by the addition of 30 μL of NaCl to see the visual color change in the dAuNPs-Tablet solution. Results indicated that only 3 mM Fe^{2+} produced aggregation while <3 mM salt was not enough to generate the radical from H_2O_2. As the radical generation is highly dependent on reaction pH, an acidic pH range of the ferrous solution was tested because at higher pH values (i.e., basic range) ferric ions precipitated as hydroxide, hence unsuitable for the Fenton reaction.[53] In our assay, the ferrous solution was prepared in citrate-phosphate buffer. The high amount of the •OH radical was produced at pH 2.5–3.0 which was selected for the H_2O_2 assay. Finally, a wide temperature range (until 50 °C) was studied for the Fenton reaction, showing the optimal temperature was 20–30 °C because the •OH radical generation was reduced at higher temperature.

3.3. Mechanism of Fenton-Assisted Oxidative Damage of the Dextran Layer around dAuNPs. In this section, we further explored the mechanism underlying the Fenton-assisted oxidative damage of the dextran layer surrounding the dAuNPs. This is with the aim of gaining insight into the processes that drive the colorimetric response observed in our plasmonic sensors. Understanding these intricate molecular interactions is essential for interpreting the sensor's performance and optimizing its sensitivity and specificity for detecting urinary H_2O_2 as an oxidative stress biomarker. Fenton-mediated colorimetric detection of H_2O_2 through •OH-assisted dextran degradation, resulting in dAuNPs aggregation, is shown in Figure 3A.

Dextran-gold nanoparticles (dAuNPs) are stable due to the electrostatic forces as well as steric hindrance caused by the long chains of polysaccharide around the nanoparticles. Oxidative damage of polysaccharide chains generates small fragments of polymer that cannot stabilize the gold colloidal suspension, hence promoting the aggregation of nanoparticles. Among different oxidative approaches, the Fenton reaction is well-known. It is worth mentioning that the incubation of a plasmonic tablet with H_2O_2 did not cause aggregation even

https://doi.org/10.1021/acsanm.4c05691
ACS Appl. Nano Mater. XXXX, XXX, XXX–XXX

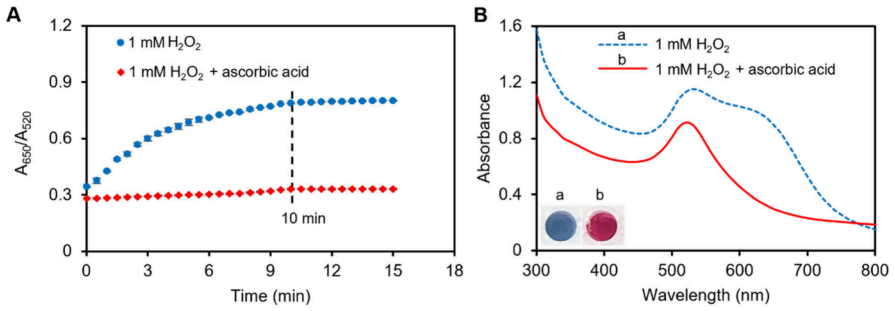

Figure 5. Kinetic study and hydroxyl radical (•OH) scavenging activity using a tablet sensor. **A)** The kinetic study for H_2O_2 detection indicates a 10 min time-window for the maximum color change of the dAuNPs probe. The presence of ascorbic acid reduces the aggregation of dAuNPs by scavenging •OH resulting in decreased A_{650}/A_{520} values; **B)** The spectral scan of the dAuNPs detection solution after 10 min when using H_2O_2 alone and with ascorbic acid. An image in the inset shows (a) aggregated dAuNPs and (b) dispersed dAuNPs.

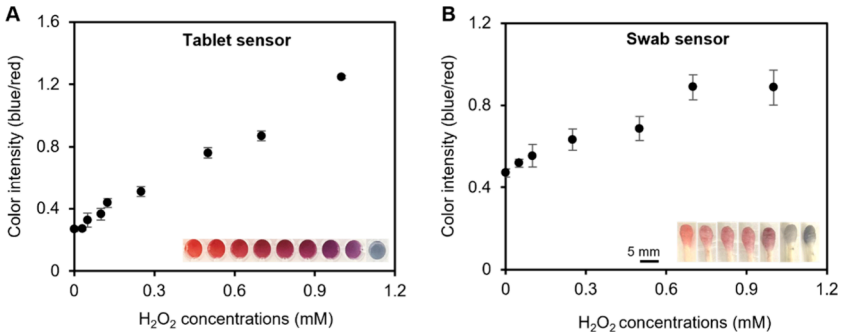

Figure 6. Plasmonic tablet and swab sensors for the colorimetric detection of H_2O_2 in artificial urine at 30, 50, 100, 125, 250, 500, 700, and 1000 μM. **A)** The calibration curve shows a linear relationship for H_2O_2 detection using the dAuNPs-Tablet. An inset shows a gradual color change of a sensing probe; **B)** The calibration curve for H_2O_2 detection using the blue/red color intensity of the dAuNPs-Swab. An inset shows the color difference in cotton swabs due to varying H_2O_2 concentrations.

when the concentration of H_2O_2 exceeded 5 M. Fenton's reagent produces the highly reactive •OH radical which initiates dextran degradation by abstracting hydrogen atom at any C−H bonds of the glucopyranose ring.[54] This hydrogen abstraction may generate a radical on the carbon atom which leads to the cleavage in either of the two directions as shown in Figure S5. If the radical is at a carbon which forms glycosidic bonds, it undergoes a β-scission reaction resulting in depolymerization of dextran chains with and/or without ring opening.[54] However, if the radical is on any carbon other than a glycosidic bond-associated carbon, it promotes the ring opening reaction leading to the formation of a carbonyl group.[55] The multiple oxidized species are produced which are relatively unspecific due to the availability of a large number of C−H bonds in the dextran chain which forms stabilized α-hydroxyalkyl radicals (·C(OH)RR′).[56] The oxidized dextran fragments are unable to stabilize the colloidal gold suspension; hence, aggregation is induced as shown in Figure 3B. Overall, the H_2O_2 detection strategy relies on •OH-mediated oxidative damage of dAuNPs followed by the distance-dependent color transition with the assistance of salt due to its signal amplifying role.

The aggregation of dAuNPs in the tablet solution and on the swab is visually apparent and evidenced by SPR peak broadening (Figure 4A), reduced ζ-potential (−10 mV and −5.9 mV, respectively) (Figure 4B), and increased hydrodynamic sizes (911 and 558 nm, respectively) (Figure 4C). TEM/SEM imaging further confirms these aggregates, highlighting the role of H_2O_2 in nanoparticle aggregation (Figure 4D-E).

3.4. A Kinetic Study and Scavenging of the •OH Radical with Ascorbic Acid. Next, by examining the rate of reaction and the effectiveness of ascorbic acid in neutralizing the radical, we aim to deepen our understanding of the antioxidant properties of this compound. This investigation is important for implications for our plasmonic sensor technology. The generation of the •OH radical in the detection system was confirmed by scavenging it with ascorbic acid due to its radical-quenching nature. In this study, ascorbic acid was incubated with Fenton's reagent to quench the •OH radical as it produced. Thus, quenching of the •OH radical inhibited the dextran degradation around dAuNPs resulting in well-dispersed stable nanoparticles. A kinetic study of H_2O_2 detection was executed using UV−vis spectroscopy as shown in Figure 5A. For this, 1 mM H_2O_2 in the presence and absence of ascorbic acid was screened for the gradual color change in the dAuNPs probe. An increase in A_{650}/A_{520} values indicated the aggregation of dAuNPs which was prominent with time. As expected, the Fenton-ascorbic acid system showed a lower value for A_{650}/A_{520} than H_2O_2 alone which indicated the capturing of the •OH radical by ascorbic acid, resulting in less aggregation of dAuNPs. In short, direct evidence for the Fenton-induced aggregation of dAuNPs was supported by ascorbic acid-induced dispersion of dAuNPs by quenching •OH. The presence of a quencher in the system inhibits the dextran degradation, hence dAuNPs remain protected. The spectrum of dAuNPs in the presence of ascorbic acid showed λ_{max} at 520 nm, representing a fully dispersed state of nanoparticles. However, the spectrum of 1

https://doi.org/10.1021/acsanm.4c05691
ACS Appl. Nano Mater. XXXX, XXX, XXX−XXX

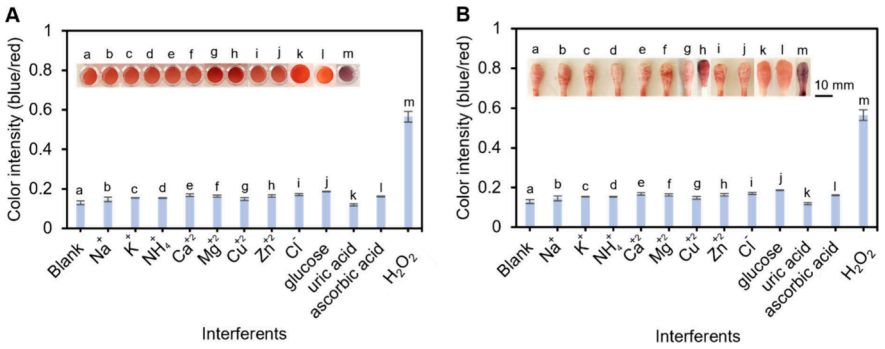

Figure 7. Selectivity test in the presence of different potential chemicals (Na^+, K^+, Mg^{2+}, NH_4^+, Ca^{2+}, Zn^{2+}, Cu^{2+}, Cl^-, glucose, uric acid, and ascorbic acid) in artificial urine. **A)** Tablet sensor shows a good selectivity toward H_2O_2 detection. The optical image in the inset shows color changes induced by corresponding interferents; **B)** A graph showing the selectivity of a swab sensor toward urinary H_2O_2 detection. The optical image in the inset shows color changes induced by corresponding interferents.

mM H_2O_2 without ascorbic acid showed a bathochromic shift due to aggregation of dAuNPs as shown in Figure 5B.

3.5. Analytical Performance of the Plasmonic Tablet and Swab Sensors. To evaluate the analytical performance of the plasmonic tablet and swab sensors, a comprehensive analysis of sensitivity, specificity, and detection limits was conducted. This evaluation is essential for determining the reliability and accuracy of our sensor technology in real-world applications, paving the way for its potential use in point-of-care diagnostics and healthcare settings. To ensure consistent imaging conditions, we captured the images of the swabs and tablet-based assay solutions using a custom-built imaging setup with controlled lighting and a fixed sample holder to maintain consistent height and angle positioning. This approach ensured the experimental integrity and reproducibility. Moreover, for a fully developed device for point-of-care settings, an opaque box can be created and integrated with smartphone imaging to provide an affordable, portable, and user-friendly solution for end users, as reported in the literature.[57] The sensitivity of the proposed plasmonic tablet and swab probe was determined against a wide concentration range of H_2O_2 in water and artificial urine as shown in Figure 6. Under the optimal conditions (10 μL of 3 mM Fe_2SO_4 solution at pH 3.0, 30 μL of 1 M NaCl, reaction temperature of 20 °C, and reaction time of 10 min), the absorbance intensity was measured for a series of H_2O_2 concentrations (30, 50, 100, 125, 250, 500, 700, and 1000 μM) in water and artificial urine. Results in water are presented in Figure S6. The calibration curve in artificial urine is achieved considering blue/red color intensity versus H_2O_2 concentrations due to •OH-induced oxidative damage of the dextran layer around nanoparticles, which promoted aggregation in dAuNPs. We observed that the sensor's response was clearly visible to the naked eye at a concentration of ≥100 μM, whereas lower concentrations required the assistance of *ImageJ* for interpretation. The LoD of the proposed sensor was calculated as the lowest concentration generated a signal that was proportional to the analyte concentration and with a value of at least three times the blank standard deviation. The tablet sensor exhibited a strong linear relationship within the range of 0.03−1.0 mM H_2O_2, with a correlation coefficient (R^2) of 0.99, as shown in Figure 6A. The linear equation for the tablet sensor is [y = 0.9412x + 0.2739]. The LoD was determined to be 50 μM in the artificial urine. Next, the swab sensor was tested for the quantitative detection of H_2O_2 within a range of 0−1000 μM as shown in Figure 6B. All experiments were repeated three times to calculate the standard deviation. The blue/red color intensity was used as ordinates, and the concentration of H_2O_2 was used as abscissa. The RGB color intensity significantly reflects the color intensity and turned to blue with the increase of H_2O_2 concentration, hence, achieving a visualized qualitative analysis of H_2O_2. The swab sensor showed a linear range of 0.05−1.0 mM H_2O_2 (R^2 = 0.93), with the corresponding linear equation being [y = 0.4322x + 0.5029]. The LoD was determined to be 100 μM in artificial urine, as depicted in Figure 6B. Notably, the calibrations for the tablet and swab sensors appear very similar (Figure 6A and 6B); however, the calculated LoDs in artificial urine are 50 μM and 100 μM, respectively. The higher LoD observed for the swab sensor can be attributed to the lower intensity of the color signal. This reduced signal intensity arises from the fibrous white structure of the cotton swab, which causes the deposited dAuNPs to blend into the white background. As a result, the color sharpness diminishes, leading to a less pronounced color change. In contrast, the lower LoD of the tablet sensor in artificial urine can be explained by the complete dissolution of the tablet in the liquid medium. This eliminates any interference from a substrate or medium, resulting in a sharp, high-intensity colorimetric signal. Additionally, the tablet-based assay demonstrated greater consistency in artificial urine, as evidenced by the lower standard deviation of the blank signal. Consequently, this led to a lower LoD based on our calculation method.

The stability of dAuNPs-Tablet and dAuNPs-Swab sensors is another important factor when considering the portability of these platforms, because such analytical devices are very likely to be stored for a certain time before being employed in the field. Our previous studies showed that the dAuNPs-Tablet is stable for >one year.[27] The plasmonic swabs after drying were placed in an airtight glass jar and stored under ambient conditions for different intervals of time. The dAuNPs impregnated cotton swab sensing characteristic remained unchanged for 1 month followed by a gradual decrease in its stability up to 40% within three months as shown in Figure S7.

Our study presents a novel, nanoparticle-based approach for the detection of H_2O_2 using dAuNPs, which offers significant advantages over traditional chromogenic reagents such as TMB (3,3′,5,5′-tetramethylbenzidine) and OPD (*o*-phenylenediamine). The traditional chromogenic reagents often present significant drawbacks, including the need for specific storage conditions, light sensitivity, high toxicity, and poor solubility as well as limitations in portability and specificity. These solutions often need to be freshly prepared before the

https://doi.org/10.1021/acsanm.4c05691
ACS Appl. Nano Mater. XXXX, XXX, XXX−XXX

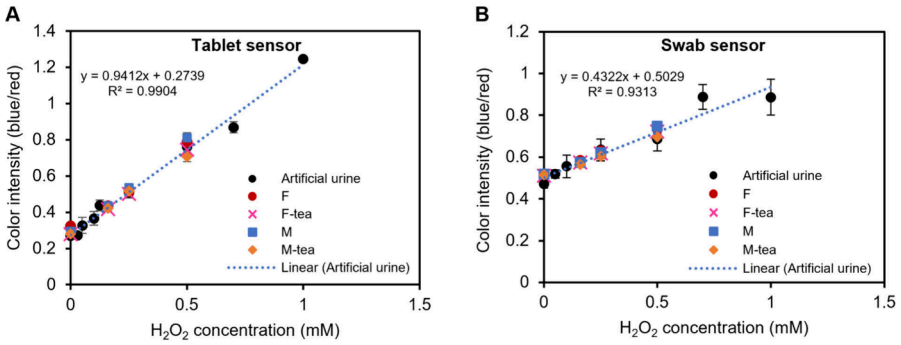

Figure 8. Real sample analysis to measure oxidative stress through a H_2O_2 assay using a plasmonic tablet and swab sensors. **A)** A spiking test was conducted using the tablet sensor in female (F) and male (M) urine samples before green tea consumption, along with F-tea and M-tea samples, which were collected after green tea intake; **B)** A spiking test with a plasmonic swab sensor was performed, showing blue/red color intensity of the swab analyzed using *ImageJ* software. Some data points are not visible on the graph due to the overlapping of data points.

experiments, making them less suitable for point-of-care diagnostics in nonlaboratory settings. In contrast, the plasmonic properties of dAuNPs enable a clear, visible color change from red to blue in the presence of H_2O_2 through the Fenton reaction. The dAuNPs-based assay is straightforward and can be easily adapted into various formats, such as tablets and swabs, enhancing portability and making it suitable for point-of-care diagnostics. Moreover, the biocompatible nature of dAuNPs broadens the applicability of our assay. Furthermore, the dAuNPs tablets demonstrated remarkable long-term stability, retaining functionality for over a year. The high selectivity of this method also ensures minimal interference from other substances, making it a robust and practical method for colorimetric H_2O_2 detection.

3.6. Selectivity of the H_2O_2 Assay. The selectivity of the proposed H_2O_2 assay was investigated using several competing metal cations (Na^+, K^+, NH_4^+, Ca^{2+}, Mg^{2+}, Zn^{2+}, Cu^{2+}), anion (Cl^-), and small organic interferents (glucose, uric acid, and ascorbic acid) using a plasmonic tablet and swab sensors as shown in Figures 7A and 7B, respectively. The interferent concentration of cations and H_2O_2 was chosen to be 1 mM, while 0.1 mM anion, glucose, uric acid, and ascorbic acid were added in artificial urine separately. It was observed that the Fenton reaction was unaffected by these interfering chemicals and generated the •OH radical successfully followed by selective detection of urinary H_2O_2. As interfering species cause negligible interferences on the aggregation of dAuNPs by the •OH radical, both tablet and swab sensors can be used to measure urinary H_2O_2 which reflects the total body oxidative stress.

3.7. Practical Application. Next, we transition from laboratory evaluations to real-world applications, exploring the practical utility of our plasmonic sensors. Our focus shifts to assessing total body oxidative stress through the analysis of urine samples collected from volunteers. Specifically, we investigate the impact of dietary interventions, such as green tea consumption, on oxidative stress levels. This real-world evaluation provides invaluable insights into the efficacy and reliability of our sensor technology in diverse physiological contexts.

The total body oxidative stress was evaluated by performing real sampling analysis against human urine samples of healthy volunteers (female and male) before and after consuming green tea for a specific period. Building upon this investigation, in a case study, we further explored the potential benefits of green tea consumption on oxidative stress levels, as green tea is renowned for its antioxidant properties and purported ability to alleviate stress. Volunteers, who were carefully selected from the same family to better maintain consistency in dietary habits throughout the study period, were instructed to consume green tea three times a day for a week, while their urine samples were collected and analyzed. The higher value of H_2O_2 in human urine is associated with different diseases including urinary tract infections, diabetes, cancer, inflammatory condition, and oxidative stress. Thus, a sensor capable of detecting urinary H_2O_2 across a wide concentration range, from low to high levels, is crucial for providing an accurate estimation of a patient's health profile. Such a sensor could offer valuable insights into oxidative stress-related conditions and help in the early diagnosis and monitoring of diseases. Female (F) and male (M) urine samples were used within 1 h of dispense and spiked with low to high concentrations of H_2O_2 (160, 200, 250, and 500 μM) followed by adopting the detection procedure (Figure 8). This range of H_2O_2 concentrations was chosen to demonstrate the assay's capability across a broad spectrum, as H_2O_2 levels can vary significantly with the progression of different disease conditions and health scenarios. The amount of H_2O_2 in the real samples analyzed in this study was below the detection limit of our sensors, and no quantifiable amounts were detected in unspiked samples. The amount found in unspiked samples was up to 40 μM by the calibration curve which is not quantifiable with our sensor. We employed the standard addition method and spiking recovery analysis, as detailed in Table S1, to evaluate the accuracy and applicability of our method. These approaches are critical for assessing potential matrix effects that may influence the analyte signal and validating the calibration curve for H_2O_2 detection. Spiking was performed at varying concentrations to rigorously test the assay's performance and demonstrate its robustness.

The R% for F and M samples were observed in the range of 91−111% and 104−118% respectively using the plasmonic tablet sensor. It is well-known that green tea reduces urinary oxidative stress due to the presence of antioxidants.[58] In this study, the same female and male volunteers consumed green tea (200 mL) three times a day for a week, and then their samples as F-tea (female urine sample after consuming green tea) and M-tea (male urine sample after consuming green tea) were spiked with similar H_2O_2 concentration. The R% was found in the range of 84−105% for F-tea and 85−107% for M-tea samples. However, green tea effectively reduced oxidative stress in both female and male. The % reduction in female

https://doi.org/10.1021/acsanm.4c05691
ACS Appl. Nano Mater. XXXX, XXX, XXX−XXX

samples ranged from 0.04 to 5.71%, whereas in male samples, it varied from 0.56 to 16.58% (Figure S8). The RSD% of the tablet sensor was in the range 0.46−4.53 for female samples and 0.84−3.74% for male samples. In addition to RGB analysis of a tablet sensor, we have recorded absorbance values for H_2O_2 detection using a UV−vis spectrophotometer, and the results are presented in Figure S9.

A similar experiment was repeated with the plasmonic swab sensor using 160, 250, and 500 μM H_2O_2 concentrations as shown in Figure 8B. The R% of female samples (F) was calculated as 105−120% without green tea and 90−111% after consuming green tea (F-tea), whereas it was observed as 92−119% for M samples and 80−103% for M-tea samples. The decrease in urinary oxidative stress was observed after consuming green tea which was a maximum of 5.41% for female samples and 10.14% for male samples. In brief, the % reduction in oxidative stress after green tea consumption was higher in male volunteers compared to female volunteers. The RSD% of all samples was in the range of 0.25−3.13% showing good precision of the dAuNPs-Swab sensor.

In conclusion, the findings indicate that consuming green tea leads to a decrease in urinary H_2O_2 levels. As illustrated in Figures 8A and 8B, the values before and after spiking in green tea samples (for both female and male subjects) are lower compared to those without green tea consumption. This suggests that the reduction in the amount of H_2O_2 in urine is due to antioxidant properties of green tea. The comparison with other H_2O_2 detection methods is summarized in Table S2. Markedly, our proposed tablet and swab sensors demonstrate the capacity to detect H_2O_2 across a wide range of concentrations, which is particularly significant in the context of disease conditions within the body. The excellent sensing performance can be attributed to (i) the highly reactive nature of the hydroxyl radical (•OH) that degrades the dextran chains attached to the dAuNPs and (ii) the small size and high dispersion of dAuNPs, which result in a pronounced color change when H_2O_2 is used as the analyte.

Colorimetric methods often have higher detection limits (μM range) compared to more sensitive techniques such as electrochemical sensors or SERS, which can achieve pM or nM levels. However, the choice of detection method depends on the application and target sample. Our tablet and swab sensor's detection limits are well-suited for detecting oxidative stress-related H_2O_2 variations in urine. Further studies on nanoparticle enhancement, e.g., using hybrid nanoparticles and functionalization, can also be conducted to enhance the limit of detection and sensitivity of the assay.[59]

4. CONCLUSION

In this study, we introduced a nanoscale-driven approach for determining urinary H_2O_2 levels as an oxidative stress biomarker utilizing two platforms: dAuNPs-Tablet and dAuNPs-Swab. Both platforms were fabricated from the colloidal solution of dextran-gold nanoparticles (dAuNPs-Sol), with postsynthetic incorporation of 2% pristine dextran to enhance nanoparticle stability at the nanoscale. The plasmonic tablet was created through drop casting, while the plasmonic swab was prepared by depositing dAuNPs onto an alkaline-treated cotton swab. H_2O_2 detection relied on the aggregation of dAuNPs, initiated by the •OH radical from H_2O_2 via the Fenton reaction. This reaction degraded the dextran chains surrounding the nanoparticles, showcasing the critical role of nanoscale interactions in the sensor response. Hence, weakly shielded dAuNPs showed aggregation upon addition of NaCl. The concentration of H_2O_2 was quantified by observing the color change of the dAuNPs probe for the tablet and swab using *ImageJ* software, a free open-source software for processing and analyzing scientific images. Calibration curves were established using various H_2O_2 concentrations in water and artificial urine, yielding a limit of detection (LoD) of 50 μM for the tablet and 100 μM for the swab sensor in urine. Meanwhile, the tablet sensor demonstrated the high stability as compared to the swab sensor which exhibited a gradual stability decline after 4 weeks.

Both nanoscale platforms demonstrated excellent selectivity for urinary H_2O_2 detection, underscoring their potential for specific oxidative stress monitoring. Their practical utility was demonstrated by testing human urine samples (both female and male) before and after green tea consumption. Results indicated a reduction in oxidative stress levels following green tea consumption, with male volunteers showing a greater reduction (up to 16.58%) compared with female volunteers (up to 5.71%). The versatility and affordability of both platforms make them promising candidates for H_2O_2 assays and potential broader applications in the detection of other reactive oxygen species (ROS). Moreover, our methodology could extend to the selective detection of ascorbic acid due to its radical scavenging activity. Overall, our nanoscale-focused approach represents an advancement in point-of-care diagnostics, contributing significantly to the field of ready-to-use colorimetric sensors and paving the way for more accessible, portable healthcare solutions.

■ ASSOCIATED CONTENT

Supporting Information

The Supporting Information is available free of charge at https://pubs.acs.org/doi/10.1021/acsanm.4c05691.

Supplemental figures S1−S9 show the characterization of dAuNPs solution, dAuNPs-Tablet, and dAuNPs-Swab; testing the suitability of different materials as a POC detection platform; optimization of experimental conditions for H_2O_2 assay using a tablet sensor; detection of H_2O_2 in water; stability profile of a plasmonic tablet and a swab sensor, comparison of H_2O_2 levels in samples before and after green tea consumption, and absorbance intensity values of a tablet sensor by UV−vis spectrophotometer; Tables S1−S2 showing recovery calculations and comparison for the H_2O_2 assay (PDF)

■ AUTHOR INFORMATION

Corresponding Author

Sana Jahanshahi-Anbuhi − *Department of Chemical and Materials Engineering, Gina Cody School of Engineering and Computer Science, Concordia University, Montréal, Québec H4B 1R6, Canada;* orcid.org/0000-0002-2191-8430; Email: sana.anbuhi@concordia.ca

Authors

Zubi Sadiq − *Department of Chemical and Materials Engineering, Gina Cody School of Engineering and Computer Science, Concordia University, Montréal, Québec H4B 1R6, Canada*

Muna Al-Kassawneh − *Department of Chemical and Materials Engineering, Gina Cody School of Engineering and*

https://doi.org/10.1021/acsanm.4c05691
ACS Appl. Nano Mater. XXXX, XXX, XXX−XXX

Computer Science, Concordia University, Montréal, Québec H4B 1R6, Canada

Seyed Hamid Safiabadi Tali − *Department of Chemical and Materials Engineering, Gina Cody School of Engineering and Computer Science, Concordia University, Montréal, Québec H4B 1R6, Canada*

Complete contact information is available at: https://pubs.acs.org/10.1021/acsanm.4c05691

Author Contributions

ZS: Conceptualization, Investigation, Methodology, Formal analysis, Validation, Prepared figures, Writing-original draft, Review and editing; **MK:** Formal analysis, Methodology; **SHST:** Review and editing, Visualization; **SA:** Conceptualization, Project administration, Supervision, Funding acquisition, Resources. All authors read and commented on the full manuscript.

Notes

The authors declare no competing financial interest.

■ ACKNOWLEDGMENTS

The authors acknowledge the Natural Sciences and Engineering Research Council of Canada (NSERC) for funding this work through a Discovery Grant and Concordia University for Concordia University Research Chair (CURC) funds for the development of Stable Bio/Chemosensors. The authors also thank Dr. Nooshin Movahed for conducting the TEM and SEM/EDS analyses at the Centre for NanoScience Research (CeNSR), Concordia University, Montreal, Canada.

■ REFERENCES

(1) Pizzino, G.; Irrera, N.; Cucinotta, M.; Pallio, G.; Mannino, F.; Arcoraci, V.; Squadrito, F.; Altavilla, D.; Bitto, A. Oxidative Stress: Harms and Benefits for Human Health. *Oxid Med. Cell Longev* **2017**, *2017*, 1−13.

(2) Raut, S. K.; Khullar, M. Oxidative Stress in Metabolic Diseases: Current Scenario and Therapeutic Relevance. *Mol. Cell. Biochem.* **2023**, *478*, 185−196.

(3) Wang, Y.; Zhang, H.; Wang, Z.; Geng, Z.; Liu, H.; Yang, H.; Song, P.; Liu, Q. Therapeutic Effect of Nerve Growth Factor on Cerebral Infarction in Dogs Using the Hemisphere Anomalous Volume Ratio of Diffusion-Weighted Magnetic Resonance Imaging. *Neural Regen Res.* **2012**, *7* (24), 1873−1880.

(4) Tsutsui, H.; Kinugawa, S.; Matsushima, S. Oxidative Stress and Heart Failure. *J. Physiol Heart Circ Physiol* **2011**, *301*, H2181−H2190.

(5) Sharifi-Rad, M.; Anil Kumar, N. V.; Zucca, P.; Varoni, E. M.; Dini, L.; Panzarini, E.; Rajkovic, J.; Tsouh Fokou, P. V.; Azzini, E.; Peluso, I.; Prakash Mishra, A.; Nigam, M.; El Rayess, Y.; Beyrouthy, M. El; Polito, L.; Iriti, M.; Martins, N.; Martorell, M.; Docea, A. O.; Setzer, W. N.; Calina, D.; Cho, W. C.; Sharifi-Rad, J. Lifestyle, Oxidative Stress, and Antioxidants: Back and Forth in the Pathophysiology of Chronic Diseases. *Front Physiol* **2020**, *11*, 694.

(6) Graille, M.; Wild, P.; Sauvain, J.-J.; Hemmendinger, M.; Guseva Canu, I.; Hopf, N. B. Urinary 8-OHdG as a Biomarker for Oxidative Stress: A Systematic Literature Review and Meta-Analysis. *Int. J. Mol. Sci.* **2020**, *21* (11), 3743.

(7) Toto, A.; Wild, P.; Graille, M.; Turcu, V.; Crézé, C.; Hemmendinger, M.; Sauvain, J.-J.; Bergamaschi, E.; Guseva Canu, I.; Hopf, N. B. Urinary Malondialdehyde (MDA) Concentrations in the General Population—A Systematic Literature Review and Meta-Analysis. *Toxics* **2022**, *10* (4), 160.

(8) Pennathur, S.; Jackson-Lewis, V.; Przedborski, S.; Heinecke, J. W. Mass Spectrometric Quantification of 3-Nitrotyrosine, Ortho-Tyrosine, and o,o'-Dityrosine in Brain Tissue of 1-Methyl-4-Phenyl-1,2,3,6- Tetrahydropyridine-Treated Mice, a Model of Oxidative Stress in Parkinson's Disease. *J. Biol. Chem.* **1999**, *274* (49), 34621−34628.

(9) Kaur, H.; Halliwell, B. Detection of Hydroxyl Radicals by Aromatic Hydroxylation. *Methods Enzymol.* **1994**, *233*, 67−82.

(10) Rosen, G. M.; Cohen, M. S.; Britigan, B. E.; Pou, S. Application of Spin Traps to Biological Systems. *Free Radic Res. Commun.* **1990**, *9* (3−6), 187−195.

(11) Kasai, H. Analysis of a Form of Oxidative DNA Damage, 8-Hydroxy-2′-Deoxyguanosine, as a Marker of Cellular Oxidative Stress during Carcinogenesis. *Mutation Research/Reviews in Mutation Research* **1997**, *387* (3), 147−163.

(12) Yuen, J. W. M.; Benzie, I. F. F. Hydrogen Peroxide in Urine as a Potential Biomarker of Whole Body Oxidative Stress. *Free Radic Res.* **2003**, *37* (11), 1209−1213.

(13) Sato, Y.; Ogino, K.; Sakano, N.; Wang, D. H.; Yoshida, J.; Akazawa, Y.; Kanbara, S.; Inoue, K.; Kubo, M.; Takahashi, H. Evaluation of Urinary Hydrogen Peroxide as an Oxidative Stress Biomarker in a Healthy Japanese Population. *Free Radic Res.* **2013**, *47* (3), 181−191.

(14) Varma, S. D.; Devamanoharan, P. S. Excretion of Hydrogen Peroxide in Human Urine. *Free Radic Res. Commun.* **1990**, *8* (2), 73−78.

(15) Preedy, V. R.; Patel, V. B. *General Methods in Biomarker Research and Their Applications*; Preedy, V. R., Patel, V. B., Eds.; Biomarkers in Disease: Methods, Discoveries and Applications; Springer Netherlands, 2018. DOI: 10.1007/978-94-007-7696-8.

(16) Dryden, G. W.; Deaciuc, I.; Arteel, G.; McClain, C. J. Clinical Implications of Oxidative Stress and Antioxidant Therapy. *Curr. Gastroenterol Rep* **2005**, *7* (4), 308−316.

(17) Watwe, V. S.; Kulkarni, S. D.; Kulkarni, P. S. Cr(VI)-Mediated Homogeneous Fenton Oxidation for Decolorization of Methylene Blue Dye: Sludge Free and Pertinent to a Wide PH Range. *ACS Omega* **2021**, *6* (41), 27288−27296.

(18) Legrini, O.; Oliveros, E.; Braun, A. M. Photochemical Processes for Water Treatment. *Chem. Rev.* **1993**, *93* (2), 671−698.

(19) Ben, W.; Qiang, Z.; Pan, X.; Chen, M. Removal of Veterinary Antibiotics from Sequencing Batch Reactor (SBR) Pretreated Swine Wastewater by Fenton's Reagent. *Water Res.* **2009**, *43* (17), 4392−4402.

(20) Rubio, C. P.; Cerón, J. J. Spectrophotometric Assays for Evaluation of Reactive Oxygen Species (ROS) in Serum: General Concepts and Applications in Dogs and Humans. *BMC Vet Res.* **2021**, *17* (1), 226.

(21) Zhang, Z.; Chen, Z.; Cheng, F.; Zhang, Y.; Chen, L. Highly Sensitive On-Site Detection of Glucose in Human Urine with Naked Eye Based on Enzymatic-like Reaction Mediated Etching of Gold Nanorods. *Biosens Bioelectron* **2017**, *89*, 932−936.

(22) Chamarro, E.; Marco, A.; Esplugas, S. Use of Fenton Reagent to Improve Organic Chemical Biodegradability. *Water Res.* **2001**, *35* (4), 1047−1051.

(23) Evans, S. A. G.; Elliott, J. M.; Andrews, L. M.; Bartlett, P. N.; Doyle, P. J.; Denuault, G. Detection of Hydrogen Peroxide at Mesoporous Platinum Microelectrodes. *Anal. Chem.* **2002**, *74* (6), 1322−1326.

(24) Chen, W.; Chen, J.; Feng, Y. Bin; Hong, L.; Chen, Q. Y.; Wu, L. F.; Lin, X. H.; Xia, X. H. Peroxidase-like Activity of Water-Soluble Cupric Oxide Nanoparticles and Its Analytical Application for Detection of Hydrogen Peroxide and Glucose. *Analyst* **2012**, *137* (7), 1706−1712.

(25) Cao, X.; Zeng, Z.; Shi, W.; Yep, P.; Yan, Q.; Zhang, H. Three-dimensional Graphene Network Composites for Detection of Hydrogen Peroxide. *Small* **2013**, *9* (9−10), 1703−1707.

(26) Liu, Q.; Huang, Y.; Wang, S.; Yang, S.; Jiang, Z.; Huang, S. Monodispersed Au Nanoparticles Decorated MoS2 Nanosheets with Enhanced Peroxidase-like Activity Based Electrochemical H2O2 Sensing for Anticancer Drug Evaluations. *Anal. Chim. Acta* **2024**, *1320*, 342996.

(27) Sadiq, Z.; Safiabadi Tali, S. H.; Jahanshahi-Anbuhi, S. Gold Tablets: Gold Nanoparticles Encapsulated into Dextran Tablets and

Their PH-Responsive Behavior as an Easy-to-Use Platform for Multipurpose Applications. *ACS Omega* **2022**, *7* (13), 11177−11189.
(28) Chen, Z.; Cao, A.; Liu, D.; Zhu, Z.; Yang, F.; Fan, Y.; Liu, R.; Huang, Z.; Li, Y. Self-Confined Dewetting Mechanism in Wafer-Scale Patterning of Gold Nanoparticle Arrays with Strong Surface Lattice Resonance for Plasmonic Sensing. *Advanced Science* **2024**, *11* (12), e2306239.
(29) Frickenstein, A. N.; Means, N.; He, Y.; Whitehead, L.; Harcourt, T.; Malik, Z.; Sheth, V.; Longacre, L.; Taffe, H.; Wang, L.; McSpadden, I.; Baroody, C.; Yang, W.; Zhao, Y. D.; Wilhelm, S. The Predictive Synthesis of Monodisperse and Biocompatible Gold Nanoparticles. *ACS Appl. Nano Mater.* **2024**, *7*, 23250.
(30) Ye, J.; Chen, Z.; Chen, W.; Zhao, Y.; Ding, C.; Huang, Y. Gold Nanoparticles Coated with Silica Shells as High-Performance Fluorescence Nanoprobe. *ACS Appl. Nano Mater.* **2024**, *7* (5), 5543−5553.
(31) Liu, X.; Huang, D.; Lai, C.; Chen, Y.; Zhou, X.; Xu, F. Functionalized Gold Nanoparticles for Visual Determination of Dopamine in Biological Fluids. *ACS Appl. Nano Mater.* **2022**, *5* (5), 7357−7364.
(32) Ishida, T.; Murayama, T.; Taketoshi, A.; Haruta, M. Importance of Size and Contact Structure of Gold Nanoparticles for the Genesis of Unique Catalytic Processes. *Chemical Reviews* **2020**, *120*, 464−525.
(33) Mitsudome, T.; Kaneda, K. Gold Nanoparticle Catalysts for Selective Hydrogenations. *Green Chem.* **2013**, *15* (10), 2636.
(34) Oszwaldowski, S. X.; Lipka, R.; Jarosz, M. Sensitive Reversed-Phase Liquid Chromatographic Determination of Hydrogen Peroxide and Glucose Based on Ternary Vanadium(V)-Hydrogen Peroxide- 2-(5-Bromo-2-Pyridylazo)-5-Diethylaminophenol System. *Anal. Chim. Acta* **2000**, *421* (1), 35−43.
(35) Tian, X.; Qin, Y.; Jiang, Y.; Guo, X.; Wen, Y.; Yang, H. Chemically Renewable SERS Sensor for the Inspection of H2O2 Residue in Food Stuff. *Food Chem.* **2024**, *438*, 137777.
(36) Han, Z.; Zhang, L.; Lu, X. Sensitive Detection of Trace Hydrogen Peroxide via Dual-Emissive Electrochemiluminescence from a Luminol/Porphyrin System: Comprehensive Innovative Experiments on Analytical Instruments for Undergraduates. *J. Chem. Educ.* **2024**, *101* (3), 1248−1256.
(37) Huang, J. Y.; Lin, H. T.; Chen, T. H.; Chen, C. A.; Chang, H. T.; Chen, C. F. Signal Amplified Gold Nanoparticles for Cancer Diagnosis on Paper-Based Analytical Devices. *ACS Sens* **2018**, *3* (1), 174−182.
(38) Agustini, D.; Caetano, F. R.; Quero, R. F.; Fracassi da Silva, J. A.; Bergamini, M. F.; Marcolino-Junior, L. H.; de Jesus, D. P. Microfluidic Devices Based on Textile Threads for Analytical Applications: State of the Art and Prospects. *Analytical Methods* **2021**, *13* (41), 4830−4857.
(39) Suhaidi, N. A.; Halmi, M. I. E.; Rashidi, A. A.; Anuar, M. F. M.; Mahmud, K.; Kusnin, N.; Gani, S. S. A.; Shukor, M. Y. A. Colorimetric Detection of Mercury (Hg2+) Using UV-Vis Spectroscopy and Digital Image Analysis Based on Gold Nanoparticles Functionalized with Bromelain Enzyme. *3 Biotech* **2023**, *13* (5), 121.
(40) Lin, W.-Z.; Yeung, C.-Y.; Liang, C.-K.; Huang, Y.-H.; Liu, C.-C.; Hou, S.-Y. A Colorimetric Sensor for the Detection of Hydrogen Peroxide Using DNA-Modified Gold Nanoparticles. *J. Taiwan Inst Chem. Eng.* **2018**, *89*, 49−55.
(41) Wu, S.; Tan, S. Y.; Ang, C. Y.; Luo, Z.; Zhao, Y. Oxidation-Triggered Aggregation of Gold Nanoparticles for Naked-Eye Detection of Hydrogen Peroxide. *Chem. Commun.* **2016**, *52* (17), 3508−3511.
(42) Al-Kassawneh, M.; Sadiq, Z.; Jahanshahi-Anbuhi, S. User-Friendly and Ultra-Stable All-Inclusive Gold Tablets for Cysteamine Detection. *RSC Adv.* **2023**, *13* (28), 19638−19650.
(43) Hajimiri, H.; Safiabadi Tali, S. H.; Al-Kassawneh, M.; Sadiq, Z.; Jahanshahi-Anbuhi, S. Tablet-Based Sensor: A Stable and User-Friendly Tool for Point-of-Care Detection of Glucose in Urine. *Biosensors (Basel)* **2023**, *13* (9), 893.
(44) Jahanshahi-Anbuhi, S.; Kannan, B.; Leung, V.; Pennings, K.; Liu, M.; Carrasquilla, C.; White, D.; Li, Y.; Pelton, R. H.; Brennan, J. D.; Filipe, C. D. M. Simple and Ultrastable All-Inclusive Pullulan Tablets for Challenging Bioassays. *Chem. Sci.* **2016**, *7* (3), 2342−2346.
(45) Sadiq, Z.; Al-Kassawneh, M.; Safiabadi Tali, S. H.; Jahanshahi-Anbuhi, S. Tailoring Plasmonic Sensing Strategies for the Rapid and Sensitive Detection of Hypochlorite in Swimming Water Samples. *Microchimica Acta* **2024**, *191* (4), 183.
(46) Al-Kassawneh, M.; Sadiq, Z.; Jahanshahi-Anbuhi, S. Pullulan-Stabilized Gold Nanoparticles Tablet as a Nanozyme Sensor for Point-of-Care Applications. *Sens Biosensing Res.* **2022**, *38*, 100526.
(47) Tang, J.; Fu, X.; Ou, Q.; Gao, K.; Man, S. Q.; Guo, J.; Liu, Y. Hydroxide Assisted Synthesis of Monodisperse and Biocompatible Gold Nanoparticles with Dextran. *Materials Science and Engineering C* **2018**, *93*, 759−767.
(48) Halliwell, B.; Long, L. H.; Yee, T. P.; Lim, S.; Kelly, R. Establishing Biomarkers of Oxidative Stress: The Measurement of Hydrogen Peroxide in Human Urine. *Curr. Med. Chem.* **2004**, *11* (9), 1085−1092.
(49) Li, Y. D.; Li, W. Y.; Chai, H. H.; Fang, C.; Kang, Y. J.; Li, C. M.; Yu, L. Chitosan Functionalization to Prolong Stable Hydrophilicity of Cotton Thread for Thread-Based Analytical Device Application. *Cellulose* **2018**, *25* (8), 4831−4840.
(50) Nath, S.; Kaittanis, C.; Tinkham, A.; Perez, J. M. Dextran-Coated Gold Nanoparticles for the Assessment of Antimicrobial Susceptibility. *Anal. Chem.* **2008**, *80* (4), 1033−1038.
(51) Sivakavinesan, M.; Vanaja, M.; Annadurai, G. Dyeing of Cotton Fabric Materials with Biogenic Gold Nanoparticles. *Sci. Rep* **2021**, *11* (1), 13249.
(52) Popovetskiy, P. S.; Bulavchenko, A. I. Determination of Effective Hydrodynamic Diameters of Biopolymer Molecules in High-Viscosity Mixtures by Photon-Correlation Spectroscopy. *Colloid J.* **2016**, *78* (2), 196−203.
(53) Zhang, M. hui; Dong, H.; Zhao, L.; Wang, D. xi; Meng, D. A Review on Fenton Process for Organic Wastewater Treatment Based on Optimization Perspective. *Sci. Total Environ.* **2019**, *670*, 110−121.
(54) Duan, J.; Kasper, D. L. Oxidative Depolymerization of Polysaccharides by Reactive Oxygen/Nitrogen Species. *Glycobiology* **2011**, *21* (4), 401−409.
(55) Pronina, E. V.; Vorotnikov, Y. A.; Pozmogova, T. N.; Solovieva, A. O.; Miroshnichenko, S. M.; Plyusnin, P. E.; Pishchur, D. P.; Eltsov, I. V.; Edeleva, M. V.; Shestopalov, M. A.; Efremova, O. A. No Catalyst Added Hydrogen Peroxide Oxidation of Dextran: An Environmentally Friendly Route to Multifunctional Polymers. *ACS Sustain Chem. Eng.* **2020**, *8* (13), 5371−5379.
(56) Rees, M. D.; Kennett, E. C.; Whitelock, J. M.; Davies, M. J. Oxidative Damage to Extracellular Matrix and Its Role in Human Pathologies. *Free Radic Biol. Med.* **2008**, *44* (12), 1973−2001.
(57) ANH-DAO, L. T.; THANH-NHO, N.; HUU-TRUNG, B.; TIEN-GIANG, N.; UT DONG, T.; QUOC-DUY, N.; QUANG-HIEU, N.; LE-VY, N.; THANH-DIEU, N. T.; TO, D. V. T.; MINH-HUY, D.; CONG-HAU, N. A Portable Colorimetric Tool Using a Smartphone Camera Applied for Determining Total Phenolic Contents in Coffee Products. *Chinese Journal of Analytical Chemistry* **2023**, *51* (3), 100228.
(58) Coimbra, S.; Castro, E.; Rocha-Pereira, P.; Rebelo, I.; Rocha, S.; Santos-Silva, A. The Effect of Green Tea in Oxidative Stress. *Clinical Nutrition* **2006**, *25* (5), 790−796.
(59) Ren, W.; Mohammed, S. I.; Wereley, S.; Irudayaraj, J. Magnetic Focus Lateral Flow Sensor for Detection of Cervical Cancer Biomarkers. *Anal. Chem.* **2019**, *91* (4), 2876−2884.

https://doi.org/10.1021/acsanm.4c05691
ACS Appl. Nano Mater. XXXX, XXX, XXX−XXX